Available online at www.sciencedirect.com
SCIENCE DIRECT®
Journal of Sound and Vibration 289 (2006) 109–129
JOURNAL OF SOUND AND VIBRATION
www.elsevier.com/locate/jsvi

Elastic resonances of a periodic array of fluid-filled cylindrical cavities embedded in an elastic matrix

S. Robert, H. Franklin, J.-M. Conoir*

Laboratoire d'Acoustique Ultrasonore et d'Electronique (LAUE), UMR CNRS 6068, Université du Havre, Place R. Schuman, 76610 Le Havre, France

Received 22 October 2003; received in revised form 13 December 2004; accepted 31 January 2005
Available online 17 June 2005

Abstract

The resonant scattering by a periodic infinite array of fluid-filled cylindrical cavities in an elastic matrix is studied. The exact reflection and transmission coefficients of the array are calculated by means of a multiple scattering formalism taking into account all the interactions between the cavities. Numerical results are next given for low frequencies for which only the longitudinal and transverse zero modes propagate. A first study based on the analysis of the transmission coefficients clearly shows that the resonances of the array can be classified into two sets: those close to the resonances of a single cavity and those due to a resonant coupling between a cavity and its nearer neighbors. The resonant coupling is due to the interaction between the whispering-gallery surface waves propagating around each cavity. In the case of cavities with very close spacing, it is observed that the dispersion curves of the waves propagating along the array can also be classified into two sets: those with a positive group velocity have cut-off frequencies that correspond to the resonances of a single cavity, those with a negative group velocity have cut-off frequencies that correspond to the resonances resulting from the strong coupling. A new method for the analysis of the resonances is presented. It is based on the properties of the scattering matrix and consists in studying the resonant eigenvalues of the scattering matrix of the array once the background is removed. For the detection of very fine resonances, as well as in the separation of several resonances very close to each other, this method proves to be more efficient than one based on the analysis of the reflection and transmission coefficients.

*Corresponding author. Tel.: +33 2 32 744 712; fax: +33 2 32 744 719.
E-mail address: jean-marc.conoir@univ-lehavre.fr (J.-M. Conoir).

0022-460X/$ - see front matter © 2005 Elsevier Ltd. All rights reserved.
doi:10.1016/j.jsv.2005.01.057

1. Introduction

When a plane wave is incident upon a periodic array of identical elastic tubes immersed in water, a multiple scattering formalism is normally used to account for all the interactions between the tubes [1–3]. In this formalism, the reflected and transmitted fields are expressed as a superposition of modal plane waves. It has been shown that some of these modes are evanescent while the others propagate [4]. Varadan et al., using the approach of the T-matrix widely presented in Ref. [5], studied similar problem for SH waves propagating through an elastic slab containing a periodic array of elastic spheres [6]. Later, Lakhatia et al. [7] studied the case of P (or longitudinal L) and SV (or transverse T) waves propagating through an array of cylindrical cavities in a slab interposed between two elastic media. In this last case they obtained a complete solution of the scattering problem by using a Fourier–Bessel mode-matching procedure particularly valid for low frequencies.

In the present work, a different procedure is followed. The multiple scattering formalism of Twersky [2] and Audoly [3] is generalized to describe the problem of a plane wave incident on a linear periodic array of fluid-filled cylindrical cavities in an infinite elastic medium. Because of the propagation of two types of waves, L and T, the reflected and transmitted fields depend on the conversion of L waves into T waves, and vice versa. A mode conversion occurs each time a wave is incident on a cavity. In order to take into account all the mode conversions due to the multiple scattering process, the multiple scattering general theory applied to an arbitrary finite number of cavities is first presented. Then, it is applied to the array consisting of fluid-filled cavities embedded in an elastic medium. Although the validity of this analytical approach does not depend on the frequency range investigated, the reflection and transmission coefficients are computed at low frequencies. The frequency range investigated corresponds to that of the propagation of the zero order mode only. The resonant behavior of the array is somewhat difficult to analyze because of the existence of a background noise produced by the cavities. In order to circumvent this difficulty, the scattering matrix associated with the array is constructed. Then, once the background has been removed as recommended by the Resonant Scattering Theory (RST) [8], the resonances are isolated from a study of the eigenvalues of the resonant matrix. The results are compared to those obtained from the behavior of the squared modulus and the phase derivative of the transmission coefficients. The procedure followed here differs from that of Ref. [9] where the eigenvalues are obtained from the transmission matrix and computed with no considerations about the background noise. As in Ref. [10], our study can be used to calculate the propagation of waves in cavity bundles by considering these as a reticular plane of diffraction gratings [11].

2. Scattering by a finite number of cavities

The geometry is given in Fig. 1. We study a two-dimensional problem for which the axes of the $2N+1$ cylindrical cavities are parallel to the z direction. Let $(d_\varepsilon, \chi_\varepsilon)$ be the polar coordinates related to the cavity ε $(-Nn \leqslant \varepsilon \leqslant N)$ centered on O_ε, (r, θ) those of the point of observation on the outside of cavities with respect to the main frame (O, x, y, z), and $(r_\varepsilon, \theta_\varepsilon)$ the polar coordinates of the point of observation P in the frame $(O_\varepsilon, x_\varepsilon, y_\varepsilon, z)$. Throughout the paper, φ and ϕ (resp. ψ) indicate scalar (resp. z component of vector) potentials, and a $e^{-i\omega t}$ time dependence, while

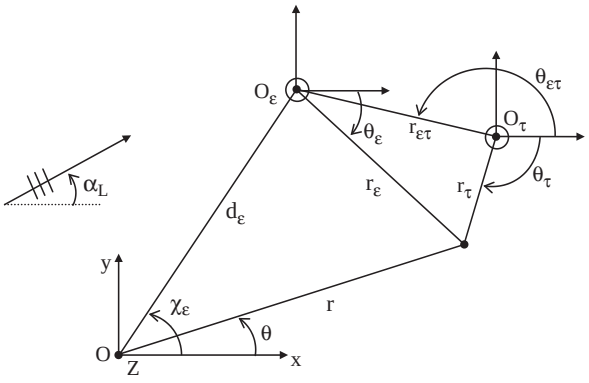

Fig. 1. Elastic scattering by a finite number of cavities: geometry.

omitted, is assumed. Let $k_L = \omega/c_L$ (resp. $k_L = \omega/c_T$) be the longitudinal L (resp. the transverse T) wavenumber, with ω the angular frequency.

A harmonic plane wave, either longitudinally or transversely polarized, is incident on all cavities. The whole longitudinal scattered field, as well as the whole transverse scattered field, are looked for. The procedure is quite simple and well-known [1–6]. Initially, the scattering properties of each single cavity ε are supposed to be known, via its scattering coefficients $T_n^{(\varepsilon)ij}$ $(i,j = L, T)$ defined below: the responses of the cavity to the incident longitudinal $(i = L)$ or transverse $(i = T)$ cylindrical field $J_n(k_i r_\varepsilon)\mathrm{e}^{\mathrm{i}n\theta_\varepsilon}$ are the scattered longitudinal field $T_n^{(\varepsilon)iL} H_n^{(1)}(k_L r_\varepsilon)\mathrm{e}^{\mathrm{i}n\theta_\varepsilon}$ and the scattered transverse field $T_n^{(\varepsilon)iT} H_n^{(1)}(k_T r_\varepsilon)\mathrm{e}^{\mathrm{i}n\theta_\varepsilon}$ ($J_n(k_i r_\varepsilon)$ denotes the Bessel function of order n and $H_n^{(1)}(k_i r_\varepsilon)$ the Hankel function of the first kind and of order n. The coefficients $T_n^{(\varepsilon)ij}$, where the subscript n denotes a mode of vibration, are obtained from the boundary conditions at the fluid/solid interface of the cavity [12]. Assuming these coefficients to be known, the whole field scattered by a finite number $2N + 1$ of cavities is expressed as the sum of the fields scattered by each cavity. This procedure was presented in a previous paper [13]. It is summarized in the following in the case of a longi-tudinal incident plane wave. Extension to the case of a transverse incident plane wave is straightforward.

Assuming the incident L wave is propagating with an incidence angle α_L, its potential can be written in the frame (O, x, y, z) as follows

$$\varphi_{\mathrm{inc}} = \mathrm{e}^{\mathrm{i}k_L r\,\cos(\theta-\alpha_L)} = \sum_{n=-\infty}^{+\infty} \mathrm{i}^n \mathrm{e}^{-\mathrm{i}n\alpha_L} J_n(k_L r)\mathrm{e}^{\mathrm{i}n\theta} = \sum_{n=-\infty}^{+\infty} a_n J_n(k_L r)\mathrm{e}^{\mathrm{i}n\theta}. \tag{1}$$

In the frame $(O_\varepsilon, x_\varepsilon, y_\varepsilon, z)$, one has

$$\varphi_{\mathrm{inc}}^{(\varepsilon)} = \sum_{n=-\infty}^{+\infty} a_n \mathrm{e}^{\mathrm{i}k_L d_\varepsilon\,\cos(\alpha_L-\chi_\varepsilon)} J_n(k_L r_\varepsilon)\mathrm{e}^{\mathrm{i}n\theta_\varepsilon} = \sum_{n=-\infty}^{+\infty} A_n^{(\varepsilon)L} J_n(k_L r_\varepsilon)\mathrm{e}^{\mathrm{i}n\theta_\varepsilon}. \tag{2}$$

The overall L and T waves scattered by cavity ε are respectively written as [6]

$$\phi_{\mathrm{s}}^{(\varepsilon)} = \sum_{n=-\infty}^{+\infty} C_n^{(\varepsilon)LL} H_n^{(1)}(k_L r_\varepsilon)\mathrm{e}^{\mathrm{i}n\theta_\varepsilon}, \quad \psi_{\mathrm{s}}^{(\varepsilon)} = \sum_{n=-\infty}^{+\infty} C_n^{(\varepsilon)LT} H_n^{(1)}(k_T r_\varepsilon)\mathrm{e}^{\mathrm{i}n\theta_\varepsilon}. \tag{3a,b}$$

In these expressions, the Hankel function of the first kind and of order n, $H_n^{(1)}$, is introduced in order to respect the Sommerfeld radiation condition. For the unknown complex coefficients $C_n^{(\varepsilon)LT}$, for instance, ε refers to the cavity, L to the nature of the incident wave and T to that of the scattered wave. It should be noted that interactions between cavities are taken into account and each coefficient $C_n^{(\varepsilon)LL}$ or $C_n^{(\varepsilon)LT}$ depends on all scattering amplitudes $T_n^{(\varepsilon)ij}$ $(-N \leqslant \varepsilon \leqslant N; i,j = L,T)$. The total acoustic fields incident on scatterer ε are then

$$\phi_{\text{inc}}^{(\varepsilon)} = \varphi_{\text{inc}}^{(\varepsilon)} + \sum_{\tau \neq \varepsilon} \phi_{\text{s}}^{(\tau)}, \quad \psi_{\text{inc}}^{(\varepsilon)} = \sum_{\tau \neq \varepsilon} \psi_{s}^{(\tau)}, \tag{4a,b}$$

where $\sum_{\tau \neq \varepsilon}$ represents the sum of the fields of the same type scattered by all other scatterers ε, except scatterer ε itself. Next, the addition theorem [14] is used to translate the basis functions from O_τ centers to the O_ε center:

$$\begin{aligned} H_n^{(1)}\left(k_j r_\tau\right) \mathrm{e}^{\mathrm{i}n\theta_\tau} &= \sum_{m=-\infty}^{+\infty} \mathrm{e}^{\mathrm{i}(n-m)\theta_{\varepsilon\tau}} H_{n-m}^{(1)}\left(k_j r_{\varepsilon\tau}\right) J_m\left(k_j r_\varepsilon\right) \mathrm{e}^{\mathrm{i}m\theta_\varepsilon} \\ &= \sum_{m=-\infty}^{+\infty} G_{nm}^{(\tau\varepsilon)j} J_m\left(k_j r_\varepsilon\right) \mathrm{e}^{\mathrm{i}m\theta_\varepsilon} \end{aligned} \tag{5}$$

with $j = L$ or T. Introducing Eq. (5) in Eqs. (4a,b), it follows that

$$\phi_{\text{inc}}^{(\varepsilon)} = \sum_{n=-\infty}^{+\infty} \left[A_n^{(\varepsilon)L} + \sum_{\tau \neq \varepsilon} \sum_{m=-\infty}^{+\infty} G_{mn}^{(\tau\varepsilon)L} C_m^{(\tau)LL} \right] J_n(k_L r_\varepsilon) \mathrm{e}^{\mathrm{i}n\theta_\varepsilon} \tag{6a}$$

and

$$\psi_{\text{inc}}^{(\varepsilon)} = \sum_{n=-\infty}^{+\infty} \left[\sum_{\tau \neq \varepsilon} \sum_{m=-\infty}^{+\infty} G_{mn}^{(\tau\varepsilon)T} C_m^{(\tau)LT} \right] J_n(k_T r_\varepsilon) \mathrm{e}^{\mathrm{i}n\theta_\varepsilon}. \tag{6b}$$

Consequently, according to the T-matrix approach [5,6], the waves scattered by scatterer ε can be written as

$$\begin{aligned} \phi_{\text{s}}^{(\varepsilon)} = &\sum_{n=-\infty}^{+\infty} T_n^{(\varepsilon)LL} \left[A_n^{(\varepsilon)L} + \sum_{\tau \neq \varepsilon} \sum_{m=-\infty}^{+\infty} G_{mn}^{(\tau\varepsilon)L} C_m^{(\tau)LL} \right] H_n^{(1)}(k_L r_\varepsilon) \mathrm{e}^{\mathrm{i}n\theta_\varepsilon} \\ &+ \sum_{n=-\infty}^{+\infty} T_n^{(\varepsilon)TL} \left[\sum_{\tau \neq \varepsilon} \sum_{m=-\infty}^{+\infty} G_{mn}^{(\tau\varepsilon)T} C_m^{(\tau)LT} \right] H_n^{(1)}(k_L r_\varepsilon) \mathrm{e}^{\mathrm{i}n\theta_\varepsilon}, \end{aligned} \tag{7a}$$

$$\begin{aligned} \psi_{\text{s}}^{(\varepsilon)} = &\sum_{n=-\infty}^{+\infty} T_n^{(\varepsilon)LT} \left[A_n^{(\varepsilon)L} + \sum_{\tau \neq \varepsilon} \sum_{m=-\infty}^{+\infty} G_{mn}^{(\tau\varepsilon)L} C_m^{(\tau)LL} \right] H_n^{(1)}(k_L r_\varepsilon) \mathrm{e}^{\mathrm{i}n\theta_\varepsilon} \\ &+ \sum_{n=-\infty}^{+\infty} T_n^{(\varepsilon)TT} \left[\sum_{\tau \neq \varepsilon} \sum_{m=-\infty}^{+\infty} G_{mn}^{(\tau\varepsilon)T} C_m^{(\tau)LT} \right] H_n^{(1)}(k_L r_\varepsilon) \mathrm{e}^{\mathrm{i}n\theta_\varepsilon}. \end{aligned} \tag{7b}$$

Comparison of Eqs. (7a,b) with respectively Eqs. (3a,b) leads to the linear system

$$C_n^{(\varepsilon)LL} - T_n^{(\varepsilon)LL} \sum_{\tau\neq\varepsilon} \sum_{m=-\infty}^{+\infty} G_{mn}^{(\tau\varepsilon)T} C_m^{(\tau)LL} - T_n^{(\varepsilon)TL} \sum_{\tau\neq\varepsilon} \sum_{m=-\infty}^{+\infty} G_{mn}^{(\tau\varepsilon)T} C_m^{(\tau)LT} = T_n^{(\varepsilon)LL} A_n^{(\varepsilon)L},$$

$$C_n^{(\varepsilon)LT} - T_n^{(\varepsilon)LT} \sum_{\tau\neq\varepsilon} \sum_{m=-\infty}^{+\infty} G_{mn}^{(\tau\varepsilon)L} C_m^{(\tau)LL} - T_n^{(\varepsilon)TT} \sum_{\tau\neq\varepsilon} \sum_{m=-\infty}^{+\infty} G_{mn}^{(\tau\varepsilon)T} C_m^{(\tau)LT} = T_n^{(\varepsilon)LT} A_n^{(\varepsilon)L}. \quad (8)$$

In the case of a plane incident T wave, one would find

$$C_n^{(\varepsilon)TL} - T_n^{(\varepsilon)LL} \sum_{\tau\neq\varepsilon} \sum_{m=-\infty}^{+\infty} G_{mn}^{(\tau\varepsilon)L} C_m^{(\tau)TL} - T_n^{(\varepsilon)TL} \sum_{\tau\neq\varepsilon} \sum_{m=-\infty}^{+\infty} G_{mn}^{(\tau\varepsilon)T} C_m^{(\tau)TT} = T_n^{(\varepsilon)TL} A_n^{(\varepsilon)T},$$

$$C_n^{(\varepsilon)TT} - T_n^{(\varepsilon)TT} \sum_{\tau\neq\varepsilon} \sum_{m=-\infty}^{+\infty} G_{mn}^{(\tau\varepsilon)T} C_m^{(\tau)TT} - T_n^{(\varepsilon)LT} \sum_{\tau\neq\varepsilon} \sum_{m=-\infty}^{+\infty} G_{mn}^{(\tau\varepsilon)L} C_m^{(\tau)TL} = T_n^{(\varepsilon)TT} A_n^{(\varepsilon)T}. \quad (9)$$

The unknown coefficients $C_n^{(\varepsilon)LL}$ and $C_n^{(\varepsilon)LT}$ (resp. $C_n^{(\varepsilon)LT}$ and $C_n^{(\varepsilon)TT}$) are found by solving the linear system (8) (resp. Eq. (9)). The overall fields scattered by the linear array are next obtained by summing all the scattered potentials $\phi_s^{(\varepsilon)}$ and $\psi_s^{(\varepsilon)}$. For a longitudinal incident plane wave, the linear array scatters the potentials

$$\phi_s = \sum_{\varepsilon=-N}^{N} \sum_{n=-\infty}^{+\infty} C_n^{(\varepsilon)LL} H_n^{(1)}(k_L r_\varepsilon) e^{in\theta_\varepsilon}, \quad \psi_s = \sum_{\varepsilon=-N}^{N} \sum_{n=-\infty}^{+\infty} C_n^{(\varepsilon)LT} H_n^{(1)}(k_T r_\varepsilon) e^{in\theta_\varepsilon}. \quad (10a,b)$$

Up to now, no assumptions on the respective positions of the cavities have been done, except that the positions were supposed to be known. The particular case of the infinite number of cavities, periodically placed in a linear array, is studied in the next section.

3. Scattering by a periodic array

The geometry of the problem is given in Fig. 2. It is assumed that all scatterers are identical and equally spaced. The array is then a periodic one. By exploiting this periodicity and by assuming at first the case of an incident L wave, one obtains

$$C_n^{(\tau)Lj} = C_n^{(\varepsilon)Lj} e^{i(\tau-\varepsilon)k_L d \sin \alpha_L} = C_n^{(\varepsilon)Lj} e^{i(\tau-\varepsilon)\varphi_L}, \quad j = L \text{ or } T, \quad (11)$$

d being the distance between the centers of two consecutive cavities. In Eq. (11), ε is the number of a given cavity, considered as a reference cavity, the choice of which being arbitrary. The following parameters are then introduced.

$$p = \tau - \varepsilon, \quad pd = r_{\varepsilon\tau}, \quad \theta_p = \theta_{\varepsilon\tau}, \quad (12)$$

with

$$\theta_p = +\pi/2 \text{ if } p<0, \quad \theta_p = -\pi/2 \text{ if } p>0. \quad (13)$$

With these notations, and using the Snell law

$$k_L \sin \alpha_L = k_T \sin \alpha_T, \quad (14)$$

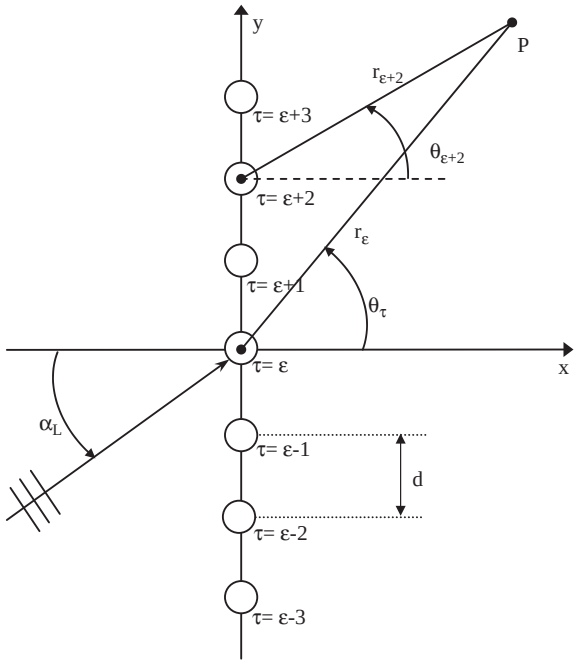

Fig. 2. Elastic scattering by a periodic array of cavities: geometry.

system (8) becomes

$$\sum_{m=-\infty}^{+\infty} \left\{ \left[\delta_{mn} - T_n^{LL} \sigma_L(m-n) \right] C_m^{LL} - T_n^{TL} \sigma_T(m-n) C_m^{LT} \right\} = T_n^{LL} A_n^{(L)},$$

$$\sum_{m=-\infty}^{+\infty} \left\{ \left[\delta_{mn} - T_n^{TT} \sigma_T(m-n) \right] C_m^{LT} - T_n^{LT} \sigma_L(m-n) C_m^{LL} \right\} = T_n^{LT} A_n^{(L)}. \tag{15}$$

In both equations of this system, δ_{mn} represents the Kronecker symbol. The superscript ε has been skipped because all scatterers are identical, and

$$\sigma_j(m-n) = \sum_{p \neq 0} H_{m-n}^{(1)}(k_j p d) \mathrm{e}^{\mathrm{i} k_j p d \sin \alpha_j} \mathrm{e}^{\mathrm{i}(m-n)\theta_p} \tag{16}$$

is the Schlömilch series [15] with $j = L$ or T. By replacing $\sum_{\varepsilon=-N}^{N}$ by $\sum_{p=-\infty}^{+\infty}$ in Eqs. (10a,b) and by taking into account that all scatterers are identical, the overall fields scattered by the array can be put in the form

$$\phi_s = \sum_{n=-\infty}^{+\infty} C_n^{LL} \Sigma_n^L, \quad \psi_s = \sum_{n=-\infty}^{+\infty} C_n^{LT} \Sigma_n^T \tag{17a,b}$$

with

$$\Sigma_n^j = \sum_{p=-\infty}^{+\infty} \mathrm{e}^{\mathrm{i} k_j p d \sin \alpha_j} H_n^{(1)}(k_j r_p) \mathrm{e}^{\mathrm{i} n \theta_p}, \quad j = L \text{ or } T. \tag{18}$$

Eq. (18) represents a sum of cylindrical waves scattered by the individual scatterers. It can be rewritten as sum of plane waves more suitable to express the array reflected and transmitted fields. To this end, a differential operator that allows to increment or decrement the index of the Hankel functions is introduced. If it is applied n times to a function (n can be as well a positive or a negative integer), one writes it

$$\Lambda^n = \frac{1}{(-k_j)^n}\left[\frac{\partial}{\partial x} + \mathrm{i}\frac{\partial}{\partial y}\right]^n \quad \text{if } n \geqslant 0, \tag{19a}$$

$$\Lambda^n = \frac{1}{k_j^{|n|}}\left[\frac{\partial}{\partial x} - \mathrm{i}\frac{\partial}{\partial y}\right]^{|n|} \quad \text{if } n < 0. \tag{19b}$$

The operators Λ^n are known as creation ($n \geqslant 0$) or annihilation ($n \leqslant 0$) operators in quantum mechanics. The relation $\Lambda^n H_0^{(1)}(k_j r_p) = H_n^{(1)}(k_j r_p)\mathrm{e}^{\mathrm{i}n\theta_p}$ can be verified straightforwardly to give

$$\Lambda^n \Sigma_0^j = \Sigma_n^j. \tag{20}$$

Next (see the Appendix), the following transformation is introduced

$$\Sigma_0^j = \sum_{p=-\infty}^{+\infty} \mathrm{e}^{\mathrm{i}k_j p d \sin\alpha_j} H_0^{(1)}(k_j r_p) = \sum_{p=-\infty}^{+\infty} \frac{2}{k_p^{(j)} d}\mathrm{e}^{\mathrm{i}\left(k_p^{(j)}|x| + \alpha_p^{(j)} y\right)} \tag{21}$$

with

$$\alpha_p^{(j)} = k_j \sin\alpha_j + \frac{2\pi p}{d} \quad \text{and} \quad k_p^{(j)} = +\left(k_j^2 - \alpha_p^{(j)^2}\right)^{1/2}. \tag{22}$$

Σ_0^j then represents a sum of plane waves. Each propagates in its own direction given by the projections $\alpha_p^{(j)}$ and $k_p^{(j)}$ of its wavevector, with either the velocity of longitudinal waves ($j = L$) or that of transverse waves ($j = T$). From Eq. (22), $\alpha_p^{(j)}$ is real, while $k_p^{(j)}$ may be complex. When $k_j < |\alpha_p^{(j)}|$, the pth plane wave is evanescent, the effective propagation being in the direction of the array (y direction) while its amplitude decays in the x direction. Otherwise, if $k_j > |\alpha_p^{(j)}|$, it is propagative. In order for the amplitude of the evanescent waves to decay as the distance of the observation point to the array is increased, one must choose, in Eq. (22), a positive imaginary part of $k_p^{(j)}$.

It follows from Eq. (20) that the right-hand side of Eq. (18) can also be expressed as a sum of plane waves

$$\Sigma_n^j = \sum_{p=-\infty}^{+\infty} \frac{2}{k_p^{(j)} d}\left[\frac{\alpha_p^{(j)} \mp \mathrm{i}k_p^{(j)}}{k_j}\right]^n \mathrm{e}^{\mathrm{i}\left(k_p^{(j)}|x| + \alpha_p^{(j)} y\right)}, \tag{23}$$

where, in the brackets, the $-$ sign corresponds to $x > 0$ and the $+$ sign to $x < 0$. Consequently, the potentials of the overall scattered fields (Eqs. (17a,b)) are put in the form

$$\phi_\mathrm{s} = \left\{\sum_{n=-\infty}^{+\infty} C_n^{LL}\Lambda^n\right\}\Sigma_0^L, \quad \psi_\mathrm{s} = \left\{\sum_{n=-\infty}^{+\infty} C_n^{LT}\Lambda^n\right\}\Sigma_0^T. \tag{24a,b}$$

The reflected and transmitted fields are both scattered fields, either evaluated at $x<0$ or at $x>0$ (see Fig. 2). In the case of an incident L wave, for instance, the reflected potentials ($j = L$ or T, $x<0$) may be finally written as

$$\phi_{\text{refl}} = \sum_{p=-\infty}^{+\infty} r_p^{LL} \mathrm{e}^{\mathrm{i}\left(-k_p^{(L)}x+\alpha_p^{(L)}y\right)}, \quad \psi_{\text{refl}} = \sum_{p=-\infty}^{+\infty} r_p^{LT} \mathrm{e}^{\mathrm{i}\left(-k_p^{(T)}x+\alpha_p^{(T)}y\right)} \tag{25a,b}$$

with

$$r_p^{Lj} = \frac{2}{k_p^{(j)} d} \sum_{n=-\infty}^{+\infty} C_n^{Lj} \left[\frac{\alpha_p^{(j)} + \mathrm{i}k_p^{(j)}}{k_L}\right]^n. \tag{26}$$

For the transmitted fields, we get

$$\phi_{\text{trans}} = \sum_{p=-\infty}^{+\infty} t_p^{LL} \mathrm{e}^{\mathrm{i}\left(k_p^{(L)}x+\alpha_p^{(L)}y\right)}, \quad \psi_{\text{trans}} = \sum_{p=-\infty}^{+\infty} t_p^{LT} \mathrm{e}^{\mathrm{i}\left(k_p^{(T)}x+\alpha_p^{(T)}y\right)} \tag{27a,b}$$

with

$$t_p^{Lj} = \delta_{p0}^{j} + \frac{2}{k_p^{(j)} d} \sum_{n=-\infty}^{+\infty} C_n^{Lj} \left[\frac{\alpha_p^{(j)} - \mathrm{i}k_p^{(j)}}{k_L}\right]^n. \tag{28}$$

In Eq. (28), δ_{p0}^{j} is defined by $\delta_{p0}^{L} \equiv \delta_{p0}$ (the Kronecker delta) and $\delta_{p0}^{T} \equiv 0$.

The equations above show that the array reflects and transmits an infinity of plane propagating or evanescent waves following different angles defined from Eq. (22). The cut-off frequencies of the linear array are the frequencies such that $k_p^{(j)} = 0$ [3]. Each value of p corresponds to two different cut-off frequencies, $f_p^{(L)}$ and $f_p^{(T)}$, satisfying $f_{p+1}^{(j)} > f_p^{(j)}$ ($j = L, T$). For frequencies less than $f_p^{(L)}$, all longitudinal modes of order p_0 propagate if $|p_0| < |p|$, and are evanescent if $|p_0| \geqslant |p|$. The two first cut-off frequencies, under which only the $p = 0$ modes L and T correspond to propagating waves, are given by

$$f_c^{(j)} = \frac{c_j}{d\left(1 + \sin\,\alpha_j\right)}, \quad j = L \text{ or } T. \tag{29}$$

These frequencies are proportional to $1/d$; the denser the array, the higher the cut-off frequencies. They are also decreasing functions of α_j. Moreover, as $c_L > c_T$, one has $f_c^T < f_c^L$. As we are only interested by the propagating $p = 0$ modes L and T in the following, computations will be expanded for frequencies less than f_c^T.

Now, then, the waves reflected by the array, as well as those transmitted, are known. Both types of waves are described as an infinite sum of plane waves, and each plane wave is indexed by the integer p. The reflection and transmission coefficients, also indexed by p (cf. Eqs. (26) and (28)), contain infinite sums over the integer n. Their effective computation requires the series to be truncated. One way to check all truncations have been correctly done is to check the conservation of energy.

4. Energy conservation laws and numerical study of the transmission through the array

4.1. Energy conservation laws

In this paper, all the reflection and transmission coefficients defined above have been computed by using the following criterion of convergence: computation of a series is stopped as soon as the moduli of two consecutive terms are less than 0.1% of the modulus of the truncated series. Moreover, the exact calculation of these coefficients has been checked by verifying step by step the energy conservation laws which are defined in this section. In addition, the energy conservation laws will help us to build the scattering matrix in Section 5. Let $\mathbf{u}$ be the displacement vector and $\boldsymbol{\sigma}$ the stress tensor. The x component of the acoustic intensity vector $\mathbf{j} = (1/2)\mathrm{Re}(-\boldsymbol{\sigma}.\dot{\mathbf{u}}^*)$ can be written, in the case of time harmonic waves where $\dot{\mathbf{u}} = -\mathrm{i}\omega\mathbf{u}$ as

$$j_x = \frac{\omega}{2}\mathrm{Im}\left(\sigma_{xx}u_x^* + \sigma_{xy}u_y^*\right). \tag{30}$$

The sign * denotes the complex conjugate, while

$$u_x = \frac{\partial\phi}{\partial x} + \frac{\partial\psi}{\partial y}, \quad u_y = \frac{\partial\phi}{\partial y} - \frac{\partial\psi}{\partial x} \tag{31a,b}$$

represent the components of the displacement vector and

$$\sigma_{xx} = -\lambda k_L^2\phi + 2\mu\left(\frac{\partial^2\phi}{\partial x^2} + \frac{\partial^2\psi}{\partial x\partial y}\right), \quad \sigma_{xy} = \mu\left(2\frac{\partial^2\phi}{\partial x\partial y} + \frac{\partial^2\psi}{\partial y^2} - \frac{\partial^2\psi}{\partial x^2}\right) \tag{32a,b}$$

are components of the stress tensor associated with a longitudinal field described by potential ϕ and a transverse field described by ψ. The constants λ and μ are the Lamé coefficients of the elastic medium. The energy flux in the increasing x direction perpendicular to the array is

$$J = \int_{-\infty}^{+\infty} j_x \,\mathrm{d}y. \tag{33}$$

In the case of an incident L wave, $\phi = \varphi_{\mathrm{inc}}$ and $\psi = 0$. If the incidence angle is α_L,

$$j_{\mathrm{inc}x} = \frac{\omega}{2}k_L^3(\lambda + 2\mu)\cos\alpha_L. \tag{34}$$

The transmitted waves are in this case $\phi = \phi_{\mathrm{trans}}$ and $\psi = \psi_{\mathrm{trans}}$. It follows from Eqs. (27), (31) and (32) that

$$j_{\mathrm{trans}\,x} = (\lambda + 2\mu)\,k_L^2\frac{\omega}{2}\sum_{p=-\infty}^{+\infty} k_p^{(L)}\left|t_p^{LL}\right|^2 + \mu k_T^2\,\frac{\omega}{2}\sum_{p=-\infty}^{+\infty} k_p^{(T)}\left|t_p^{LT}\right|^2. \tag{35}$$

For the reflected waves, we get similarly, from Eqs. (25), (31) and (32)

$$j_{\mathrm{refl}\,x} = -(\lambda + 2\mu)k_L^2\frac{\omega}{2}\sum_{p=-\infty}^{+\infty} k_p^{(L)}\left|r_p^{LL}\right|^2 - \mu k_T^2\frac{\omega}{2}\sum_{p=-\infty}^{+\infty} k_p^{(T)}\left|r_p^{LT}\right|^2. \tag{36}$$

Now, the expression of the flux balance

$$J_{\mathrm{inc}} + J_{\mathrm{refl}} = J_{\mathrm{trans}} \tag{37}$$

with J_{inc}, J_{refl} and J_{trans} obtained by using Eq. (33) and the appropriate j_x defined above, leads to the energy conservation law for an incident L wave

$$\sum_{p=-\infty}^{+\infty}\left(\frac{k_p^{(L)}}{k_0^{(L)}}\left|r_p^{LL}\right|^2+\frac{k_p^{(T)}}{k_0^{(L)}}\left|r_p^{LT}\right|^2+\frac{k_p^{(L)}}{k_0^{(L)}}\left|t_p^{LL}\right|^2+\frac{k_p^{(T)}}{k_0^{(L)}}\left|t_p^{LT}\right|^2\right)=1, \tag{38}$$

with $k_0^{(L)}=k_L\cos\alpha_L$. The energy conservation law, for an incident T wave and an incidence angle α_T, is obtained the same way ($k_0^{(T)}=k_T\cos\alpha_T$):

$$\sum_{n=-\infty}^{+\infty}\left(\frac{k_p^{(L)}}{k_0^{(T)}}\left|r_p^{TL}\right|^2+\frac{k_p^{(T)}}{k_0^{(T)}}\left|r_p^{TT}\right|^2+\frac{k_p^{(L)}}{k_0^{(T)}}\left|t_p^{LL}\right|^2+\frac{k_p^{(T)}}{k_0^{(L)}}\left|t_p^{LT}\right|^2\right)=1. \tag{39}$$

4.2. Numerical study of the transmission through the array

Throughout the paper, the numerical studies are performed for an array of water-filled cavities embedded in an aluminum matrix with the following parameters: density $\rho=2700\,\text{kg/m}^3$, longitudinal velocity $c_L=6380\,\text{m/s}$ and transverse velocity $c_T=3140\,\text{m/s}$. The water parameters, density $\rho_w=1000\,\text{kg/m}^3$ and sound velocity $c_w=1494\,\text{m/s}$, are contained in the single scattering coefficient $T_n^{(\varepsilon)ij}$ previously mentioned in Section 2. Scattering by a single cavity is a function of $x_L=k_La$, with a the radius of the cavities. The period of the array is $d=\beta a$. As the cut-off frequencies are inversely proportional to d, the frequency dependence of the behavior of the array may be wholly described by its dependence on x_L. This is the reason why all figures will be plotted versus x_L. Whatever the frequency and the incidence angle, energy conservation has been numerically verified with less than 0.001% error. Moreover, we found that only the propagating modes p need to be taken into account, in Eqs. (38) and (39). This is rather logical, as evanescent waves do not carry energy in the x direction (an evanescent wave propagates in the y direction, while its amplitude decays in the x direction).

The following study has been performed for low frequencies, such that only the $p=0$ modes are propagating waves. Each transmitted field in Eqs. (27a,b), then, is a sum of only one propagating wave and an infinite number of evanescent ones. However, provided the result is evaluated far enough from the array itself, only the propagating waves need to be taken into account in the calculation of either the transmitted fields, or the reflected ones. Four transmission coefficients of the array, then, may be determined, which are t_0^{LL}, t_0^{LT}, t_0^{TL}, and t_0^{TT}.

4.2.1. Comparison of squared moduli and phase derivatives of the transmission coefficient

We have studied the squared modulus and the derivative with respect to frequency of the phase (simply called the phase derivative below) of the transmission coefficient t_0^{LL}. The squared modulus of the transmission coefficient is a quantity which can be straightforwardly obtained from an experimental measurement. This is the reason why it has been investigated first. In addition, many investigators detect resonances from the peaks of the modulus of the transmission coefficient. The phase derivative of the transmission coefficients is also studied because it has been shown that it is an even more efficient tool for the detection of resonances. This tool is based on the study of the dynamics of the phase of the transmission coefficients with regard to the frequency. However, the phase derivative is easier to use theoretically than experimentally [16].

Our first effort has been to compare the results obtained from the squared modulus of the transmission and from the phase derivative. The case of the incident L wave with $\alpha_L = 0^\circ$ is shown in Figs. 3 and 4 for two different distances between the cavities: $\beta = 2.05$ and $\beta = 3$. The respective first cut-off frequencies f_c^T then correspond to $x_L = 1.03$ and $x_L = 1.51$. For $\beta = 2.05$, resonances in Fig. 3 can be classified into two sets: those close to the resonances of a single cavity, called 'single cavity resonances, their values of which are $x_L = 0.42$, 0.70, 0.89, 0.96, 1.16, 1.25, 1.42; and those pointed at $x_L = 1.39$ and $x_L = 1.49$ on both sides of $x_L = 1.42$. As predicted, they are clearly observed in Fig. 4. In addition, the two single-cavity resonances $x_L = 1.16$ and $x_L = 1.25$ observed in Fig. 3 are seen to be split each into two others. A similar phenomenon can be observed for $\beta = 3$. For a given resonance, the comparison of the two curves shows the following phenomenon: the narrower the peak of the resonance in Fig. 3, the higher the amplitude of the phase derivative in Fig. 4. If the amplitude of the phase derivative at a maximum is denoted by $2/\gamma$, the half-width Γ measured in Fig. 3 is such that $\Gamma \geqslant \gamma$. For the resonance at $x_L = 0.42$ one has $\Gamma \simeq 0.048$ and $\gamma \simeq 0.044$ ($2/\gamma \simeq 45.3$), while for $x_L = 0.70$, $\Gamma \simeq 0.01$ and $\gamma \simeq 0.009$ ($2/\gamma \simeq 215$). The relation $\Gamma \geqslant \gamma$ is due to the fact that peaks in Fig. 3, even isolated, have not really a resonance curve shape because the transmission coefficient is perturbed by the so-called background discussed in Section 5. By derivating the phase, a part of the perturbation (the slowly varying part due to the background) becomes negligible. So, it appears to us that the values of γ are more representative of the resonance half-widths than those of Γ.

4.2.2. *The splitting of resonances*

For a finite linear array of elastic shells immersed in a fluid, the splitting of resonances has already been observed at low frequency [17]. In such a case, the resonances of a single shell that split are all related to the bending A wave [18]. This phenomenon is called resonant interaction. It is not surprising to observe a resonant interaction in the frequency range where the bending A wave circumnavigates a single shell. The energy of this wave is known to be mainly localized in the

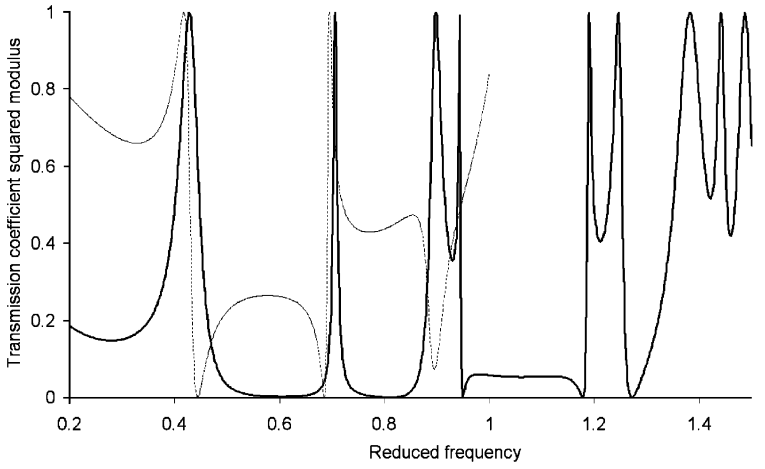

Fig. 3. Squared modulus of the transmission coefficient t_0^{LL} plotted versus the reduced frequency x_L for two distances between the cavities: $\beta = 2.05$ (in solid line) and $\beta = 3$ (in dotted line); $\alpha_L = 10^\circ$.

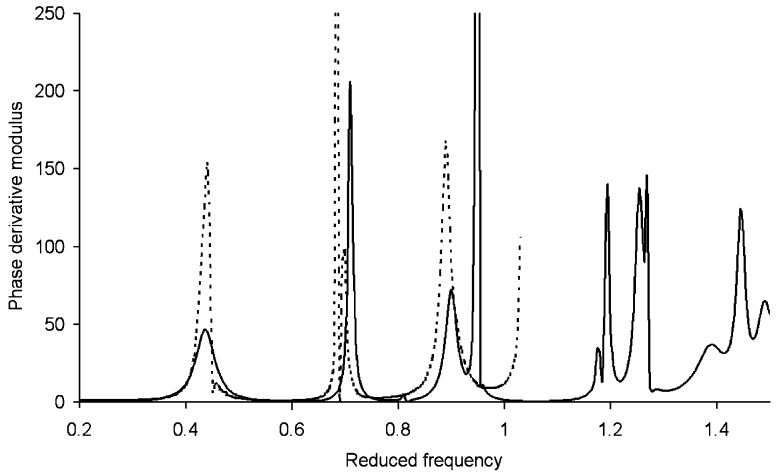

Fig. 4. Modulus of the phase derivative of t_0^{LL} plotted versus x_L for $\beta = 2.05$ (in solid line) and $\beta = 3$ (in dotted line); $\alpha_L = 10^\circ$.

surrounding fluid. Consequently, the bending A wave (one bending A wave propagates around each shell of the finite linear array) can interact as the distance between the shell axes diminishes.

In a previous paper [13], it was shown that resonant interactions also occur for a finite number of water-filled cavities embedded in a solid, with the emergence of a large number of resonances due to the splitting of the resonances of a single cavity. Resonances of a single cavity occur each time a whispering-gallery surface wave [12] circumnavigates the cavity with such a phase velocity that an integer number of wavelengths fits over its circumference. However, the strong reemission of the energy from the cavities into the solid gives rise to unknown resonant coupling mechanisms that are much more complicated than in the fluid case previously discussed. Properties of the whispering-gallery surface waves are less known than those of the bending A wave. In our opinion, the splitting of resonances observed in Fig. 4 for the periodic infinite array of fluid-filled cavities embedded in a solid is also due to a strong coupling between the cavities caused by the whispering-gallery surface waves.

Two points are worth underlining. Firstly, a resonant interaction takes place especially for a small distance between the cavities. This leads us to classify the resonances of the array into two sets : those close to single cavity resonances and those due a resonant coupling between each cavity and its nearer neighbors. Secondly, the splitting of resonances always happens around the single-cavity resonances. For $\beta = 2.05$, both resonances at $x_L = 1.16$ and at $x_L = 1.25$ are split into two, and resonance at $x_L = 1.42$ is split into three. One reason why the scattering matrix formalism is introduced later is to clarify this phenomenon.

4.2.3. Dispersion curves obtained by using the phase derivatives

In the following, the resonances will be studied with the phase derivative of the transmission coefficients, rather than from their squared moduli. In order to get an overview of the resonant properties of the array, the phase derivative of the transmission coefficients $t_0^{LL}$and $t_0^{LT}$are plotted in Figs. 5 and 6 versus both the reduced frequency and the incidence angle, for $\beta = 2.05$. In this

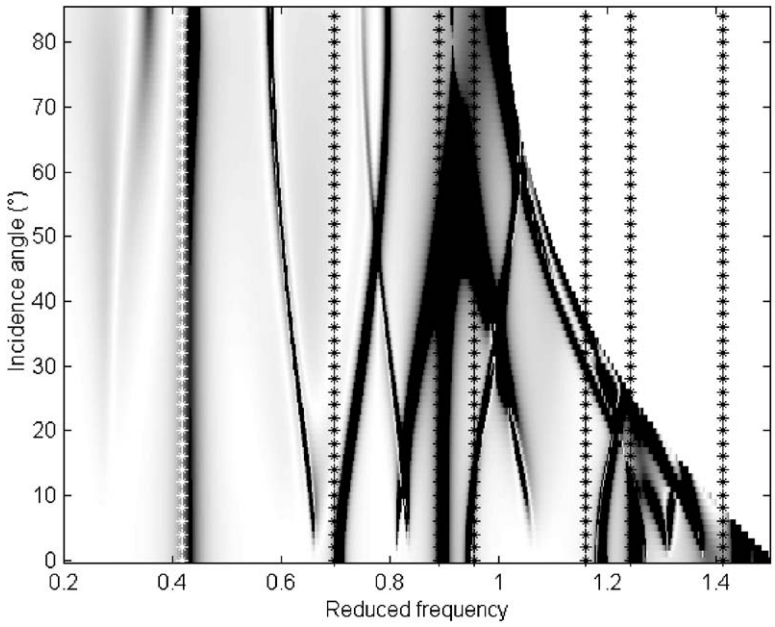

Fig. 5. Modulus of the phase derivative of t_0^{LL} plotted versus x_L and the incidence angle α_L for $\beta = 2.05$; the resonance positions of a single water-filled cavity are indicated by vertical lines with stars.

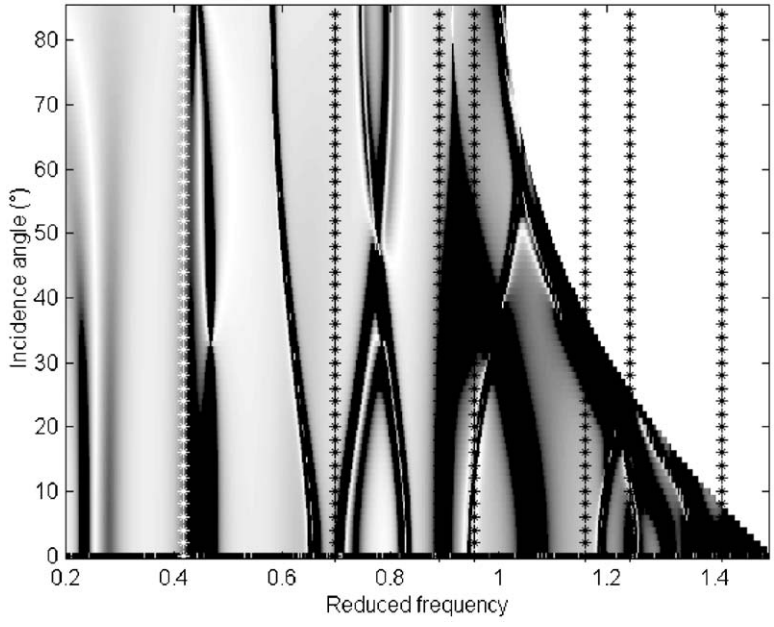

Fig. 6. Modulus of the phase derivative of t_0^{LT} plotted versus x_L and the incidence angle α_L for $\beta = 2.05$; the resonance positions of a single water-filled cavity are indicated by vertical lines with stars.

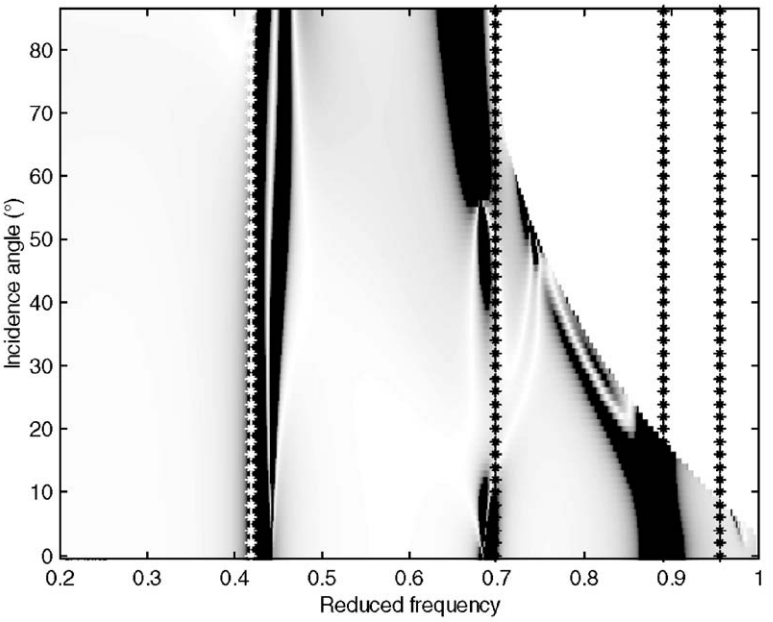

Fig. 7. Modulus of the phase derivative of t_0^{LL} plotted versus x_L and the incidence angle α_L for $\beta = 3$; the resonance positions of a single water-filled cavity are indicated by vertical lines with stars.

case, the cavities of the array are close to each other. The maxima of the phase derivative (which point out the resonance frequencies) draw black curves on the diagrams. One can note that the resonant behavior of the array is rather complicated, particularly in the vicinity of the cut-off frequency. Generally speaking, the phase derivatives of the two transmission coefficients show the same resonant behavior, except in the frequency range $0.2 \leqslant x_L \leqslant 0.3$ where an additional resonance is detected for the t_0^{LT} transmission coefficient. The other transmission coefficients (t_0^{TL} and t_0^{TT}) show similar results. The vertical dotted lines in Figs. 5 and 6 indicate the resonance frequencies of a single cavity. For small incidence angles ($\alpha_L \leqslant 10^\circ$), most of them are also resonances of the array. This result confirms that the resonances of the single cavity play a great role in the resonant behavior of the array. When the distance between cavities is larger ($\beta = 3$), as in Fig. 7, all the resonances of the array are simply single cavity resonances. For very close cavities ($\beta = 2.05$) and large enough incidence angles ($\alpha_L \geqslant 10^\circ$), the resonant coupling is reinforced. Clearly, there are new resonances which are not detected at small incidence angles.

The curves in Figs. 5–7 can also be interpreted in terms of dispersion curves associated to waves propagating along the array. As for Lamb waves in elastic plates [19], the excitation angle θ of these waves is related to k'_y, the real part of the complex wavenumber $k_y = k_L \sin \alpha_L + 2n\pi/d$ that characterizes the propagation in the y direction, as follows

$$\sin \theta = \frac{k'_y}{k_L}. \tag{40}$$

The phase velocity c_{ph} of the waves is classically given by $k'_y = \omega/c_{ph}$. Consequently, we get the relation between θ and c_{ph}, namely $\sin \theta = c_L/c_{ph}$. Two types of dispersion curves are observed in

Figs. 5 and 6 according to the sign of the group velocity. The waves with a cut-off frequency corresponding to a single-cavity resonance have always a positive group velocity. On the contrary, most of the other dispersion curves, those with a cut-off frequency that does not correspond to a single-cavity resonance, show a negative group velocity. It is worth to note that there is no repulsive phenomenon when the curve of one type of wave meets one of the other type. The dispersion curves intersect. It is not surprising because the energies of the corresponding waves propagate in opposite directions along the array. From the wave propagation point of view, this is certainly the most interesting phenomenon. Unfortunately, even for the simpler case of Lamb waves propagating in elastic plates, the reason why waves have a negative group velocity is not well understood.

As a conclusion to this section, the resonances of the array can be classified into two sets, those of a single cavity, and those due to a coupling between the cavities. Most eigenmodes of the array have a negative group velocity.

5. Scattering matrix for the array $p = 0$ mode

The curves we have plotted so far are rather complicated to use for a precise analysis of resonances, for which both the position and the width have to be determined. For a simpler structure such as an elastic plate in water, it has been shown that the eigenvalues of the scattering matrix make easier the physical interpretation of the reflection and transmission coefficients of the plate [20]. Proceeding in the same way, the computations of the eigenvalues of the scattering matrix of the array should, theoretically, supply us with more information. Unfortunately, in the present case, the problem is more difficult, because the resonant behavior of a single cavity or of an array in an elastic medium is widely masked by a background. So, it is rather difficult to obtain accurate values of the resonance frequencies. One of the key moments of the resonant scattering theory (RST) is the separation of the field scattered by an elastic object into two components [8], namely, the background and the resonant component. The background varies slowly with frequency, while the resonant component varies fast. Isolation of the resonant component may be achieved in different ways. The simplest method consists in removing, from the considered scattered field, the field that would be scattered by a reference scatterer. This field is the background. The skill required is in choosing that background, i.e. the reference scatterer. In early applications of the RST to acoustics [8], two different reference scatterers were considered: the rigid one (Neumann boundary condition) and the soft one (Dirichlet boundary condition). No waves can penetrate into such scatterers, and it was assumed that they could not give rise to resonances. In order to explain the physical meaning of the background, it is useful to discuss the scattering process in terms of geometric and surface waves. Consider, for example, the scattering by a single fluid-filled cavity. There are the specularly longitudinal and transverse reflected waves, which are geometric type waves, the creeping (or Franz) waves and the peripheral elastic waves, which are surface waves circumnavigating the cavity. Scattering by a rigid or a soft scatterer gives rise to the reflected and creeping waves only. It has been shown that if the background chosen is correct, the reflected and creeping waves of the reference scatterer practically coincide with those of the elastic scatterer. Then, after removal of the background from the field scattered by the elastic object, the only contribution left is that of the peripheral elastic waves, which are

responsible for the resonances. According to the RST, the only way to remove the background is to factorize the scattering matrix $\mathbf{S} = \mathbf{S}^{(0)}\mathbf{S}^{(*)}$, with $\mathbf{S}^{(0)}$ associated with the background and $\mathbf{S}^{(*)}$ with the resonant component of the field. The next step, then, is the construction of the scattering matrix $\mathbf{S}$ of the array.

5.1. Scattering matrix of the array

As before, the frequency range investigated is such that only the zero modes are propagating waves. The main property of the scattering $\mathbf{S}$ matrix is its unitarity ; this is due to energy conservation. So, our first step in the construction of the $\mathbf{S}$ matrix will be deduced from energy conservation laws, Eqs. (38) and (39), established in Section 4.1, in which the infinite summation may be reduced to the $p = 0$ terms

$$\left|r_0^{LL}\right|^2 + \frac{k_0^{(T)}}{k_0^{(L)}}\left|r_0^{LT}\right|^2 + \left|t_0^{LL}\right|^2 + \frac{k_0^{(T)}}{k_0^{(L)}}\left|t_0^{LT}\right|^2 = 1, \tag{41}$$

$$\frac{k_0^{(L)}}{k_0^{(T)}}\left|r_0^{TL}\right|^2 + \left|r_0^{TT}\right|^2 + \frac{k_0^{(L)}}{k_0^{(T)}}\left|r_0^{TL}\right|^2 + \left|r_0^{TT}\right|^2 = 1. \tag{42}$$

The following relationships between coefficients hold (they can be verified from computations):

$$x_0^{TL} r_0^{LT} = \frac{1}{x_0^{TL}} r_0^{TL}; \quad x_0^{TL} t_0^{LT} = -\frac{1}{x_0^{TL}} t_0^{TL} \tag{43}$$

with

$$x_0^{LT} = \sqrt{\frac{k_0^{(L)}}{k_0^{(T)}}} = \frac{1}{x_0^{TL}}. \tag{44}$$

The problem consists now in building a matrix $\mathbf{S}$ that verifies the following unitarity condition [21]

$$\mathbf{S}\mathbf{S}^{+} = \mathbf{S}^{+}\mathbf{S} = \mathbf{I}_d, \tag{45}$$

where $+$ denotes the hermitic conjugation and $\mathbf{I}_d$ the identity matrix. Of course, $\mathbf{S}$ will be well defined if Eq. (45) involves Eqs. (41) and (42). The most natural way to solve this problem is to introduce a matrix that takes into account the mode conversions between the L and T type waves

$$\mathbf{S} = \begin{bmatrix} \mathbf{S}_0^{LL} & \mathbf{S}_0^{TL} \\ \mathbf{S}_0^{LT} & \mathbf{S}_0^{TT} \end{bmatrix}, \tag{46}$$

where each component $\mathbf{S}_0^{ij}$ ($i,j = L$ or T) is a (2×2) submatrice defined as

$$\mathbf{S}_0^{ij} = x_0^{ij} \begin{bmatrix} r_0^{ij} & t_0^{ij} \\ t_0^{ij} & r_0^{ij} \end{bmatrix}, \tag{47}$$

with $x_0^{ij} = 1$ if $i = j$. First, it is easy to show analytically that Eq. (45) involves Eqs. (41) and (42). Then, the unitary character of the $\mathbf{S}$ matrix defined in Eq. (46) has been checked numerically. Two general properties of unitary matrices in addition to Eq. (45) are: (i) the eigenvalues have absolute

value unity, (ii) the associated eigenvectors define an orthonormal basis. Consequently, the $\mathbf{S}$ matrix can be put in the diagonal form $\mathbf{S}_{\text{diag}}$.

5.2. Numerical results

In order to remove the background, the S matrix is factorized:

$$\mathbf{S} = \mathbf{S}^{(0)}\mathbf{S}^{(*)} \tag{48}$$

with $\mathbf{S}^{(0)}$ the scattering matrix related to the array made up of empty cavities and $\mathbf{S}^{(*)}$ the resonant matrix. In this way, the simple interactions due to the reflections between two neighboring cavities, which are almost the same for empty cavities as for fluid-filled ones, are cancelled. Such a choice of the background leads to keep only the fluid–solid interactions for the multiple scattering analysis. Then, the $\mathbf{S}^{(*)}$ matrix is diagonalized. Its eigenvalues are the roots of a characteristic polynomial of degree four which cannot be factorized easily. Although it would be possible to obtain those roots analytically, we have searched them numerically to avoid numerous square root determinations. A (4×4) diagonal matrix $\mathbf{S}^{(*)}_{\text{diag}}$ is then obtained, from which is constructed another diagonal matrix, the resonant $\mathbf{T}^{(*)}_{\text{diag}}$ matrix [5]:

$$\mathbf{T}^{(*)}_{\text{diag}} = \frac{1}{2i}\left(\mathbf{S}^{(*)}_{\text{diag}} - \mathbf{I}_d\right). \tag{49}$$

The squared moduli of the elements of this new matrix are plotted versus frequency in Figs. 8 and 9. Fig. 8 corresponds to $\beta = 3$ and $\alpha_L = 0^\circ$. This curve shows a series of well-shaped Breit–Wigner curves [22]. As established by the RST, each peak corresponds to a resonance. The most interesting result is that the splitting of resonances, already observed in Fig. 4, is much better shown here. In Fig. 4 (dotted lines), there is only one resonance around $x_L = 0.9$, while there are

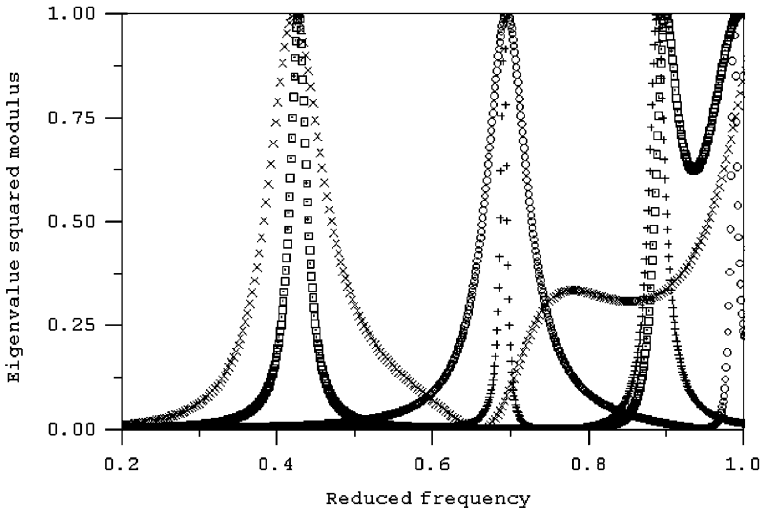

Fig. 8. Squared moduli of the four eigenvalues of the scattering matrix $\mathbf{S}^{(*)}$ of the array plotted versus x_L for $0.2 \leqslant x_L \leqslant 1$ with $\beta = 3$.

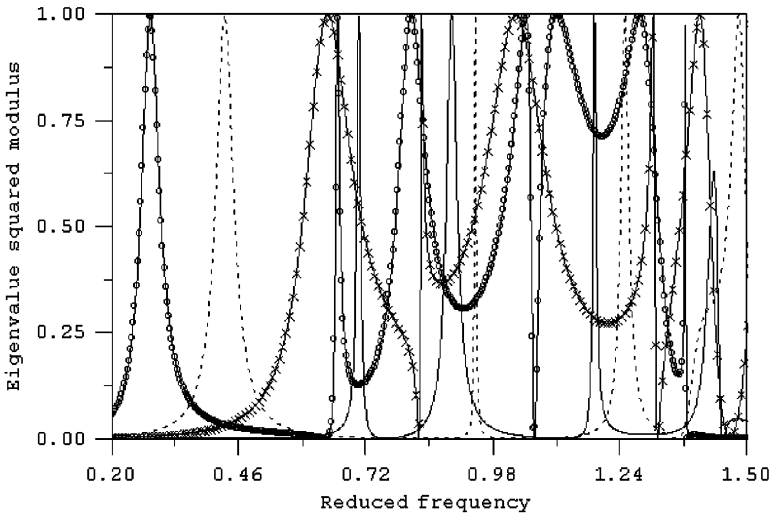

Fig. 9. Squared moduli of the four eigenvalues of the scattering matrix $\mathbf{S}^{(*)}$ of the array plotted versus x_L for $0.2 \leqslant x_L \leqslant 1.5$ with $\beta = 2.05$.

two of them in Fig. 8. However, in Fig. 8, we got rid of the background and the two resonances do no more overlap as in Fig. 4. The second curve considered corresponds to $\beta = 2.05$ and $\alpha_L = 10^\circ$. Fig. 9 shows the evolution with regard to the frequency of the squared moduli of the elements of $\mathbf{T}^{(*)}_{\text{diag}}$. As previously, a series of well shaped Breit–Wigner curves is observed. Once more, comparison with Figs. 5 and 6 shows that a few resonances, detected from the analysis of the resonant eigenvalues, are not observed on the phase derivative curves, because of the interference effect due to the background. It is interesting to compare the half-widths Γ_{BF} obtained in Fig. 9 with the half-widths γ furnished by the phase derivative plotted in Fig. 4. For $x_L = 0.42$, $\Gamma_{BF} \simeq 0.043$ and $\gamma \simeq 0.044$ while for $x_L = 0.70$, $\Gamma_{BF} \simeq 0.009$ and $\gamma \simeq 0.009$. Actually, after computation of the resonance half-widths, one finds the relation $\Gamma_{BF} \leqslant \gamma \leqslant \Gamma$. This leads to conclude that for most of the resonances, Γ_{BF} furnishes the best estimation.

As a conclusion of this section, from a theoretical point of view, the study of the resonant eigenvalues is the best tool for analyzing the resonant behavior of the array.

6. Conclusion

A multiple scattering formalism for an array of fluid-filled cylindrical cavities has been presented. The reflection and transmission coefficients have been computed at low frequencies where only the longitudinal and transverse zero modes propagate.

A first resonance study, based on the analysis of the transmission coefficients, reveals that the resonances of the array can be separated into the single-cavity resonances and the ones resulting from a resonant coupling between each cavity and its close neighbors. The dispersion curves of the waves propagating along the array have been classified into two sets. Those with a positive group

velocity have cut-off frequencies that correspond to the single-cavity resonances. Those with a negative group velocity have cut-off frequencies that corres-pond to the resonances resulting from the strong coupling.

The resonances have been studied by analyzing the scattering matrix eigenvalues of the array. The background noise produced by the cavities has been removed by following the Resonant Scattering Method (RST). It appears that the use of the resonant eigenvalues is a much more powerful method than the one based on analysis of the transmission coefficients. It allows us to detect very thin resonances as well as to separate two resonances that are very close to each other. However, from an experimental point of view, it is again not possible to obtain the resonant eigenvalues. This is the reason why it remains of interest to study the transmission coefficients, and especially the derivative with regard to the frequency of their phases, which is the more efficient method to detect resonances in this case.

Appendix

The Hankel function $H_0^{(1)}(k_j r_\varepsilon)$ is the solution of the nonhomogeneous Helmholtz equation

$$\left(\nabla^2 + k_j^2\right) H_0^{(1)}(k_j r_p) = 4\mathrm{i}\delta(x)\delta(y - pd), \tag{A.1}$$

in which $\nabla^2 = \partial^2/\partial x^2 + \partial^2/\partial y^2$ denotes the Laplacian and $\delta(\bullet)$ the Dirac distribution. From Eq. (A.1) and the Poisson sum formula, one deduces [1] that

$$\left(\nabla^2 + k_j^2\right) \Sigma_0^j = \frac{4\mathrm{i}}{d}\delta(x) \sum_{p=-\infty}^{+\infty} \mathrm{e}^{\mathrm{i}k_j y \alpha_p^{(j)}}, \tag{A.2}$$

with $\alpha_p^{(j)} = \sin\alpha_j + 2\pi p/k_j d$. The physical solution v_p^j of the partial differential equation

$$\left(\nabla^2 + k_j^2\right) v_p^j = 4\mathrm{i}\delta(x)\mathrm{e}^{\mathrm{i}k_j y \alpha_p^{(j)}} \tag{A.3}$$

being

$$v_p^j = \frac{2}{k_p^{(j)} d} \mathrm{e}^{\mathrm{i}(k_p^{(j)}|x| + \alpha_p^{(j)} y)} \tag{A.4}$$

with $k_p^{(j)} = \left(k_j^2 - \alpha_p^{(j)2}\right)^{1/2}$, one can write

$$\Sigma_0^j = \sum_{p=-\infty}^{+\infty} v_p^j \tag{A.5}$$

which represents the right-hand side of Eq. (21). Here, the choice of the positive determination for $k_p^{(j)}$ leads to

$$\lim_{|x| \to +\infty} \Sigma_0^j = 0 \tag{A.6}$$

and ensures that evanescent plane waves are scattered by the array.

For Σ_n^j, one applies the operator Λ^n, Eqs. (19a,b), to the Hankel function $H_0^{(1)}(k_j r_p)$ to give $H_n^{(1)}(k_j r_p)\mathrm{e}^{\mathrm{i}n\theta_p}$. It then follows that

$$\Lambda^n \Sigma_0^j = \Sigma_n^j. \tag{A.7}$$

Eq. (23) is now proved by considering separately the cases $x>0$ and $x<0$. If $x>0$, Eq. (A.5) becomes

$$\Sigma_{0+}^j = \sum_{p=-\infty}^{+\infty} \frac{2}{k_p^{(j)} d}\, \mathrm{e}^{\mathrm{i}\left(k_p^{(j)} x + \alpha_p^{(j)} y\right)} \tag{A.8}$$

and one obtains, after having applied Λ^n to Σ_{0+}^j:

$$\Sigma_{n+}^j = \sum_{p=-\infty}^{+\infty} \frac{2}{k_p^{(j)} d} \left[\frac{\alpha_p^{(j)} - \mathrm{i}k_p^{(j)}}{k_j}\right]^n \mathrm{e}^{\mathrm{i}\left(k_p^{(j)} x + \alpha_p^{(j)} y\right)}. \tag{A.9}$$

If $x<0$, one has analogously

$$\Sigma_{n-}^j = \sum_{p=-\infty}^{+\infty} \frac{2}{k_p^{(j)} d} \left[\frac{\alpha_p^{(j)} + \mathrm{i}k_p^{(j)}}{k_j}\right]^n \mathrm{e}^{\mathrm{i}\left(-k_p^{(j)} x + \alpha_p^{(j)} y\right)}. \tag{A.10}$$

By unifying Eqs. (A.9) and (A.10), Eq. (23) is found.

References

[1] V. Twersky, On the scattering of waves by an infinite grating, *IEEE Transactions on Antennas and Propagation AP* 4 (1956) 330–345.

[2] V. Twersky, On the scattering of waves by the infinite grating of circular cylinders, *IRE Transactions on Antennas and Propagation* 10 (1962) 737–765.

[3] C. Audoly, G. Duméry, Modelling of compliant tube underwater reflectors, *Journal of the Acoustical Society of America* 87 (1990) 1841–1846.

[4] P.C. Waterman, Scattering by periodic surfaces, *Journal of the Acoustical Society of America* 57 (1975) 791–802.

[5] V. K. Varadan, Multiple scattering of acoustic, electromagnetic and elastic waves, in: *Acoustic, Electromagnetic and Elastic Wave Scattering. Focus on the T-matrix Approach*, Pergamon, New York, 1980 pp. 103–134.

[6] V.K. Varadan, V.V. Varadan, Y.H. Pao, Multiple scattering of elastic waves by cylinders of arbitrary cross section. I. SH wave analysis, *Journal of the Acoustical Society of America* 63 (1978) 1310–1319.

[7] A. Lakhtakia, V.V. Varadan, V.K. Varadan, Reflection characteristics of an elastic slab containing a periodic array of circular elastic cylinders: P and SV wave analysis, *Journal of the Acoustical Society of America* 83 (1988) 1267–1275.

[8] L. Flax, L.R. Dragonette, H. Überall, Theory of elastic resonance excitation by sound scattering, *Journal of the Acoustical Society of America* 63 (1978) 723–731.

[9] L.S. Mulholland, M.A. Heckl, Multi-directional sound wave propagation through a tube bundle, *Journal of Sound and Vibration* 179 (1) (1994) 37–62.

[10] C. Audoly, G. Duméry, Acoustic wave propagation in media containing two-dimensional periodically spaced elastic inclusions, in: O. Leroy, M.A. Breazeale (Eds.), *Physical Acoustics*, Plenum Press, New York, 1991, pp. 199–204.

[11] M.A. Heckl, Sound propagation in bundles of periodically arranged cylindrical tubes, *Acustica* 77 (1992) 143–152.

[12] S.G. Solomon, H. Überall, K.B. Yoo, Modes conversion and resonance scattering of elastic waves from a cylindrical fluid-filled cavity, *Acustica* 55 (1984) 147–159.

[13] S. Robert, J.-M. Conoir, H. Franklin, F. Luppé, Resonant elastic scattering by a finite number of cylindrical cavities in an elastic matrix, *Wave Motion* 40 (2004) 225–239.
[14] M. Abramowitz, I.A. Stegun, *Handbook of Mathematical Functions*, Dover Publications, New York, 1964, p. 363.
[15] V. Twersky, Elementary functional representations of Schlömilch series, *Archives of Rational Mechanics Analysis* 8 (1961) 323–332.
[16] S. Derible, P. Rembert, J.-L. Izbicki, Experimental determination of acoustic resonance width via the Argand diagram, *Acustica* 84 (1998) 270–279.
[17] S. Lethuillier, J.-M. Conoir, P. Pareige, J.-L. Izbicki, Resonant acoustic scattering by a finite linear array of elastic shells, *Ultrasonics* 41 (2003) 655–662.
[18] N.D. Veksler, J.-L. Izbicki, J.-M. Conoir, Bending A wave in the scattering by a circular cylindrical shell: its relation with the bending free modes, *Journal of the Acoustical Society of America* 96 (1994) 287–293.
[19] I.A. Viktorov, *Rayleigh Lamb Waves*, Plenum Press, New York, 1967.
[20] H. Franklin, E.B. Danila, J.-M. Conoir, S-matrix theory applied to acoustic scattering by asymmetrically fluid-loaded elastic isotropic plates, *Journal of the Acoustical Society of America* 110 (1) (2001) 243–253.
[21] P.C. Waterman, Matrix theory of elastic wave scattering, *Journal of the Acoustical Society of America* 60 (1976) 567–580.
[22] G. Breit, E.P. Wigner, Capture of slow neutrons, *Physical Review* 49 (1936) 519–531.